

Article

The Novel Application of Optimization and Charge Blended Energy Management Control for Component Downsizing within a Plug-in Hybrid Electric Vehicle

Ravi Shankar *, James Marco and Francis Assadian

Department of Automotive Engineering, School of Engineering, Cranfield University, College Road, Cranfield, Bedfordshire, MK43 0AL, UK; E-Mails: j.marco@cranfield.ac.uk (J.M.); f.assadian@cranfield.ac.uk (F.A.)

* Author to whom correspondence should be addressed; E-Mail: r.shankar@cranfield.ac.uk; Tel.: +44-123-475-4648; Fax: +44-123-475-8259.

Received: 21 August 2012; in revised form: 30 October 2012 / Accepted: 16 November 2012 / Published: 23 November 2012

Abstract: The adoption of Plug-in Hybrid Electric Vehicles (PHEVs) is widely seen as an interim solution for the decarbonization of the transport sector. Within a PHEV, determining the required energy storage capacity of the battery remains one of the primary concerns for vehicle manufacturers and system integrators. This fact is particularly pertinent since the battery constitutes the largest contributor to vehicle mass. Furthermore, the financial cost associated with the procurement, design and integration of battery systems is often cited as one of the main barriers to vehicle commercialization. The ability to integrate the optimization of the energy management control system with the sizing of key PHEV powertrain components presents a significant area of research. Contained within this paper is an optimization study in which a charge blended strategy is used to facilitate the downsizing of the electrical machine, the internal combustion engine and the high voltage battery. An improved Equivalent Consumption Method has been used to manage the optimal power split within the powertrain as the PHEV traverses a range of different drivecycles. For a target CO₂ value and drivecycle, results show that this approach can yield significant downsizing opportunities, with cost reductions on the order of 2%–9% being realizable.

Keywords: PHEV; battery; energy management; equivalent consumption minimization strategy (ECMS); component sizing; optimization

Abbreviations

AER	All Electric Range
APU	Auxiliary Power Unit
Batt	Battery
BSFC	Brake Specific Fuel Consumption
CAN	Controller Area Network
CB	Charge Blending
CD	Charge Depleting
CO ₂	Carbon Dioxide
CS	Charge Sustaining
DOT	Department of Transport
DOD	Depth of Discharge
DP	Dynamic Programming
ECMS	Equivalent Consumption Minimization Strategy
EOL	End of Life
EPA	Environment Protection Agency
EU	European Union
EV	Electric Vehicle
GPS	Global Positioning System
HEV	Hybrid Electric Vehicle
HV	High Voltage
ICE	Internal Combustion Engine
INV	Inverter
NEDC	New European Driving Cycle
NN	Neural Network
PHEV	Plug-in Hybrid Electric Vehicle
PI	Proportional plus Integral Controller
PSAT	Powertrain Systems Analysis Toolkit
SoC	State of Charge
SoC _{init}	Initial State of Charge
Trn	Transmission
UNECE	United Nations Economic Commission for Europe
US	United States

Notations

F_r	Total resistive force on the tyre (N)
H_l	Lower heating value of fuel (J/kg)
M_v	Total mass of the vehicle (kg)
N_{cyl}	Number of strokes per cycle (-)
P_{aux}	Power drawn by the ancillaries (W)

P_b	Power provided by the battery (W)
$P_{bat(peak)}$	Peak power of the battery (W)
P_{dmd}	Power demand (W)
$P_{em(peak)}$	Peak power of the electric machine (W)
P_{em}	Power drawn by the electric machine (W)
$P_{em(scaled)}$	Scaled peak power of the electric machine (W)
$P_{ice(peak)}$	Peak power of internal combustion engine (W)
P_{ice}	Power provided by the ICE (W)
Q_b	Capacity of the battery (Ah)
Q_{cell}	Capacity of the individual cell (Ah)
R_b	Resistance of the battery pack (Ω)
R_{cell}	Resistance of an individual cell (Ω)
R_{int}	Internal Resistance of the battery (Ω)
T_e	Torque of the engine (Nm)
T_{em}	Torque of the electric machine (Nm)
$T_{em(base)}$	Torque of the base electric machine map (Nm)
$T_{em(scaled)}$	Scaled torque of the electric machine (Nm)
T_w	Torque at the wheels (Nm)
V_d	Volumetric size of the engine (m^3)
c_{me}	Mean piston speed (m/s)
g_{fd}	Final drive gear ratio(-)
i_b	Battery current (A)
m_f	Mass of fuel (kg)
m_c	Mass of the chassis (kg)
m_{bat}	Mass of the battery (kg)
m_{em}	Mass of electrical machine (kg)
m_{ice}	Mass of the ICE (kg)
p_{loss}	Mechanical loss in terms of pressure (Pa)
p_{me}	Mean effective pressure (Pa)
p_{mf}	Mean fuel pressure (Pa)
r_w	Radius of the wheel (m)
v_{oc}	Open circuit voltage of the battery pack
$v_{oc(cell)}$	Open circuit voltage of an individual cell
v_t	Terminal voltage at the battery (V)
η_e	Efficiency of the engine (-)
η_{em}	Efficiency of the electric machine (-)
ω_e	Engine speed (rad/s)
ω_{em}	Speed of the electric machine (rad/s)
S	Stroke length (m)
e	Thermodynamic efficiency (-)
$grav$	Acceleration due to gravity ($9.81 m/s^2$)
np	Number of parallel strings

ns	Number of cells in series
v	Vehicle velocity (km/h)
α	Slope of the road (-)
β	Power split ratio
ζ	Equivalence ratio for battery fuel consumption (-)

1. Introduction

Within the automotive and road transport sector, one of the main drivers for technological development and innovation is the need to reduce the vehicle's fuel consumption and the emissions of carbon dioxide (CO₂) [1]. Legislative requirements are motivating manufacturers and subsystem suppliers to develop new and innovative electric vehicles (EV) and hybrid electric vehicle (HEV) concepts. In recent years, plug-in hybrids (PHEV) have also attracted considerable interest from both academia and industry.

The adoption of PHEVs or *range extended EVs* is widely seen as an interim solution for the decarbonization of the transport sector [2]. Augmenting the electrical components of the powertrain with a small internal combustion engine (ICE) helps to overcome the limited range of existing EVs [3]. This improvement in range can be achieved without significant financial investment for new recharging infrastructure or a step-change improvement in the energy density of the storage technology being required [1,2].

Within a traditional series HEV the inclusion of the energy storage device, allows the ICE to be decoupled from the load acting on the vehicle. As a result, the ICE is able to operate for longer periods within a higher efficiency region or along the best specific fuel consumption (BSFC) line. The inclusion of a plug-in capability means that the state of charge (SoC) of the battery can be replenished through connection of the vehicle to the electrical grid. Therefore negating the need for the vehicle to employ a charge sustaining (CS) energy management control strategy.

The distance a PHEV can travel using only the battery is typically known as the vehicle's all electric range (AER). Typical AER values can range from 32–64 km (20–40 miles) [4]. If the vehicle is operating in a charge depleting mode (CD) and for journeys that are shorter than the AER of the vehicle, then the PHEV will have zero tank-to-wheel CO₂ emissions. However, recognizing that one of the primary drivers for the adoption of PHEVs is the ability to use the vehicle for travelling extended distances, the design challenge is one of:

- (1) correctly sizing the powertrain components for hybrid operation; and
- (2) managing the energy flows between the ICE and the battery so as to maximize operating efficiency and the reduction of CO₂ tail-pipe emissions.

With respect to powertrain component sizing, correctly determining the required energy storage capacity of the high voltage (HV) battery remains one of the primary concerns for vehicle manufacturers and system integrators [5]. This fact is particularly pertinent since the HV battery constitutes the single largest contributor to vehicle mass [6]. Furthermore, the financial cost associated with the

procurement, design and integration of large battery systems within vehicles is cited within [7] as one of the main barriers to vehicle commercialization.

For journey distances in excess of the quoted AER, the traditional method of managing the energy flows with the powertrain is for the PHEV to be driven in a CD mode until the battery SoC has depleted to a lower threshold, before transitioning to a CS mode in which the ICE is used to maintain the SoC within the required range. However, research published in [8–10] advocates a third mode of operation, namely the charge blended (CB) mode in which both the ICE and the electrical subsystems are optimally employed throughout the journey. As discussed in [11] because the ICE is able to operate in its most efficient region for comparatively longer an overall reduction in energy consumption and CO₂ emissions can be realized.

A fundamental requirement for the design and implementation of a CB strategy within a PHEV is the correct identification of the *split* of power between the ICE and the HV battery. A number of publications cite different approaches that include the use of heuristic rule-based controllers through to advanced control techniques based on optimization, fuzzy logic and game theory [7,12].

The application of more advanced control methods to solve the energy management problem opens up a number of possibilities. Discussed in [11] is the potential for higher levels of CO₂ reduction through the use of an *improved* Equivalent Consumption Minimization Strategy (ECMS) for energy management. The improvement within the design relates to the novel integration of a proportional plus Integral (PI) controller within the ECMS strategy to calculate the charge sustaining penalty function. This approach extends previously published work in which the penalty function is mainly represented by a pre-calculated steady-state look-up table. The research highlights that a CB approach combined with the local cost function optimization strategy may yield tank-to-wheel CO₂ reductions in the order of 4%–10%, when compared to the performance of traditional heuristic based control systems.

While continued CO₂ reduction constitutes the primary driver for a significant proportion of transport related research, the objective of this paper is to critically evaluate the use of the improved ECMS as a means of reducing the financial cost of key PHEV components. Consideration is constrained to the primary elements of the powertrain, namely the combined ICE and generator, the HV battery and finally the electrical machine.

A scalable model of PHEV powertrain has been designed to support system optimization and the evaluation of different energy management techniques. As part of the simulation and optimization study, the PHEV model is exercised over three separate drivecycles; the New European Drivecycle (NEDC), the Artemis Cycle and a real-world cycle. For each drivecycle, the PHEV model is parameterized with an appropriate size of electrical machine and battery so it can achieve an AER of 48, 64, 80 and 96 km (30, 40, 50 and 60 miles) respectively. It is noteworthy, that this initial parameterization involves the integrated optimization of the PHEV powertrain components and the calibration thresholds for a heuristic, rule-based, control system operating in both CD and CS modes. The resultant CO₂ output for each PHEV provides a target energy consumption for use within the second optimization study discussed in this paper. For the same drivecycles and corresponding CO₂ emissions, the latter study quantifies the opportunities for component downsizing and financial cost reduction from using the improved ECMS.

This paper is structured as follows: Section 2 introduces the drivecycles employed to evaluate the performance of the PHEV model. Section 3 discusses the design of the scalable PHEV plant model.

Section 4 provides an overview of both the heuristic and improved ECMS of energy management. Section 5 presents the framework designed to optimize the respective PHEV powertrains for both tank-to-wheel CO₂ emissions and financial cost. Consideration is given to the selection of the optimization algorithm employed and the structure of the cost functions used. Results are presented in Section 6 and highlight the variation in PHEV powertrain cost and component sizes as a function of the different drivecycles, the target level of CO₂ emissions and finally the method of energy management control employed. Discussion and Conclusions are presented in Sections 7 and 8.

2. Drivecycles Employed

Three different drivecycles were employed as part of the analysis; the NEDC, the Artemis cycle and a real-world mixed urban-highway cycle recorded as part of the evaluation of the Smart Move 2 trial [13]. Appendix A1 shows the speed traces of the drivecycles employed. The slope data recorded during the trial has been ignored since current legislative requirements define that tests are performed with no additional external force [14]. Appendix A2 provides a short overview of the EV trial program, including a description of the Smart ED vehicle and the parameters recorded. Pertinent information relating to each drivecycle is presented in Table 1. For each drivecycle, four optimization studies have been undertaken using the framework presented Section 5. For each optimization run, the AER of the PHEV was changed from 48, 64, 80 and finally 96 km (30, 40, 50 and 60 miles). Each of these AER values is classified as Design Cases 1, 2, 3 and 4 respectively.

As discussed in Section 4, when considering the application of a CB strategy within a PHEV, the term AER is no longer applicable. Within the context of the results presented in this research, the baseline for comparison between the different energy management approaches is the equivalent CO₂ production over the drivecycle.

Table 1. Characterization of the different drivecycles.

Parameters	NEDC	Real-World	Artemis
Distance	10.93 km	29.83 km	73.02 km
Top Speed	33.33 m/s	28.04 m/s	36.60 m/s
Maximum Acceleration	1.04 m/s ²	3.23 m/s ²	2.86 m/s ²
Number of repetitions	10	7	2
Total distance covered	109.32 km	208.81 km	146.04 km

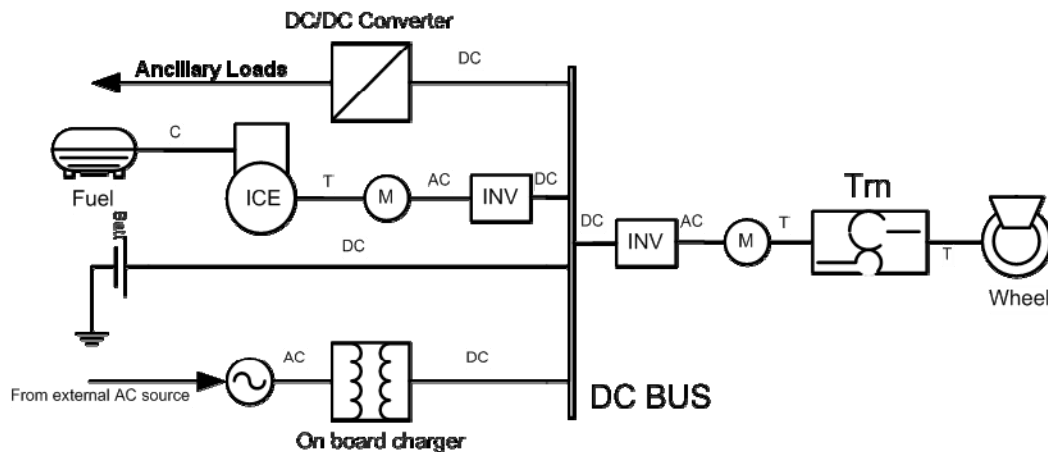
3. Design of a Scalable PHEV Model to Support System Optimization

In order to evaluate the component downsizing opportunities associated with the use of the improved ECMS strategy, an important pre-requisite is the design of a PHEV powertrain model. To facilitate an efficient optimization study, a set of low fidelity component models have been derived. The primary components of the drivetrain, namely the vehicle mass, HV battery, electrical machine and the ICE are represented by their, steady-state, non-linear efficiency characteristics.

Figure 1 presents the PHEV powertrain architecture under investigation. The on-board charger, battery (Batt), electric machine (EM), Inverters (INV), Transmission (Trn), DC/DC converter and wheel have all been modeled using data recorded from the Smart Move 2 Vehicle Trial Program. A

detailed description of this process and validation of the models has been published previously in [13,15] and will therefore not be repeated here. For each powertrain component the model execution equations have been listed. Further, for each of the powertrain components, the discussion is extended to highlight how key system parameters may be *scaled* as part of the optimization study to enable component resizing.

Figure 1. Layout of the PHEV powertrain.



The scalable parameters chosen for the PHEV model are engine volumetric size (V_d), peak power of electric machine ($P_{em(peak)}$) and the number of parallel battery strings (n_p). The sequence of execution of the model is given in Figure 2. Stage 1 consists of loading the baseline data obtained from the EV trial. Stage 2 represents the generation of a scaled set of PHEV components. Stage 3 relates to loading the different drivecycles and updating the mass of the PHEV based on the respective component mass values. Stage 4 is the execution of the model for a selected control strategy and drivecycle. Finally, Stage 5 verifies that the component constraints are maintained throughout the simulation. The remainder of the section defines in greater detail, the methods and equations involved at each stage of the process when generating and executing a scalable PHEV model.

3.1. Vehicle Model

The first part of this sub section introduces the model execution equations (Stage 4). In the second part the calculation of the mass of the powertrain components is depicted (Stage 3).

In order to calculate the resistive forces (F_r) acting on the mass of the vehicle a vehicle coast down curve was experimentally obtained for the Smart ED. Equation (1) presents the 3rd order polynomial that defines F_r as a function of vehicle speed (v). The constant term of 146.8 N represents the tire rolling resistance. The slope of the terrain (α) could be calculated using the measured height data obtained from the vehicle's onboard GPS. However, during the simulations performed in this paper the value of α was always considered to be zero:

$$F_r = (8 \times 10^{-5}) \cdot v^3 + (0.0241) \cdot v^2 + (0.1456) \cdot v + 146.8 \cdot \cos(\alpha) \quad (1)$$

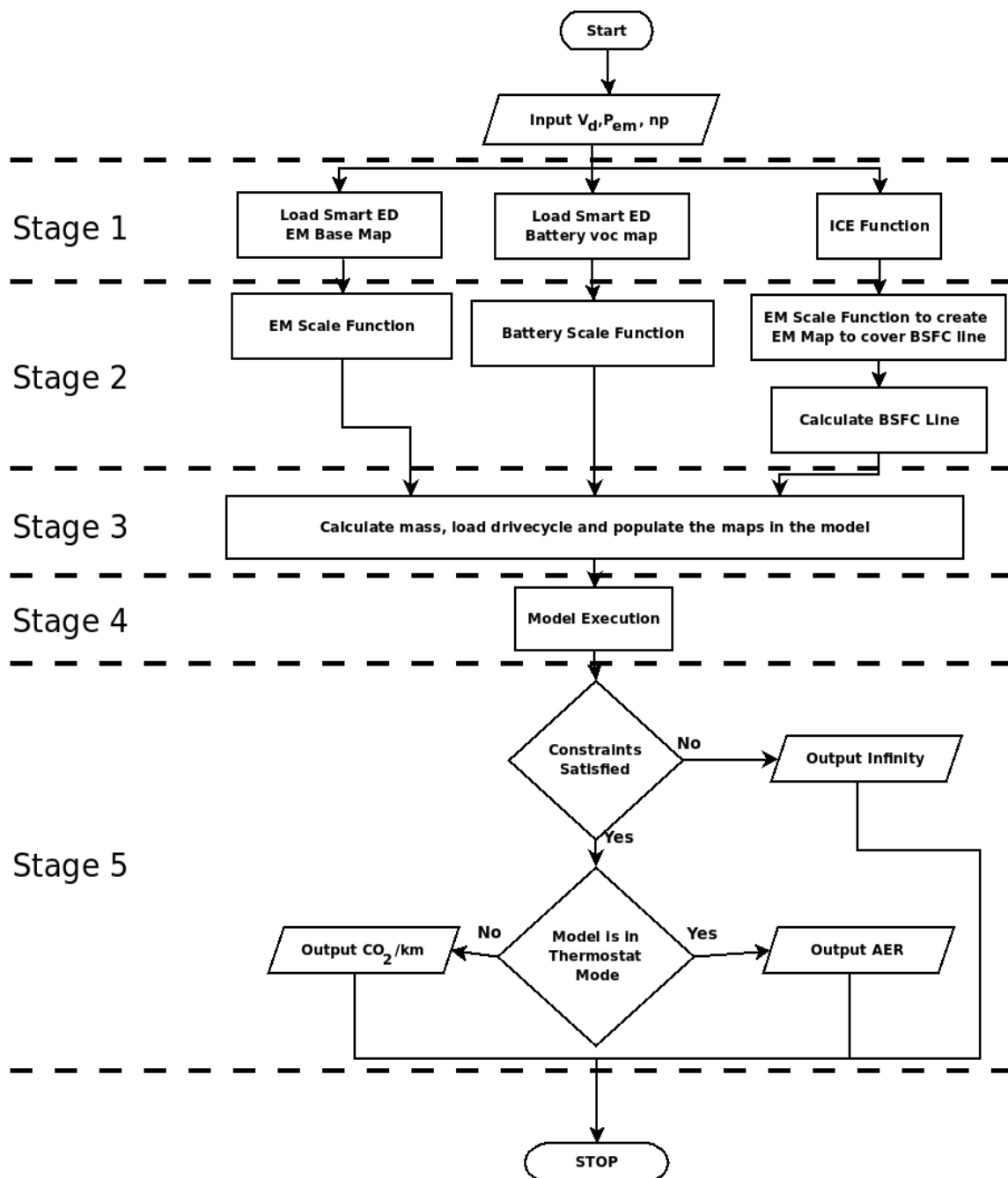
For a given vehicle speed, the associated torque at the wheels (T_w) is calculated using Equation (2), where r_w defines the rolling radius of the wheel, g is the gravitational constant and M_v is the total vehicle mass:

$$T_w = \left(M_v \cdot \frac{dv}{dt} + F_r + M_v \cdot grav \cdot \sin(\alpha) \right) \cdot r_w \quad (2)$$

The value of M_v is calculated before the execution of the model at Stage 3 of the simulation as the summation of the chassis mass (M_c), and the respective mass contributions from the electrical machine (M_{em}), battery (M_{bat}), and the ICE (M_{ice}). The mass of the vehicle chassis is held constant at 700 kg:

$$M_v = M_c + M_{em}(P_{em(peak)}) + M_{bat}(P_{bat(peak)}) + M_{ice}(P_{ice(peak)}) \quad (3)$$

Figure 2. Flowchart of execution of the simulation.



3.2. Integrated Electric Machine and Transmission

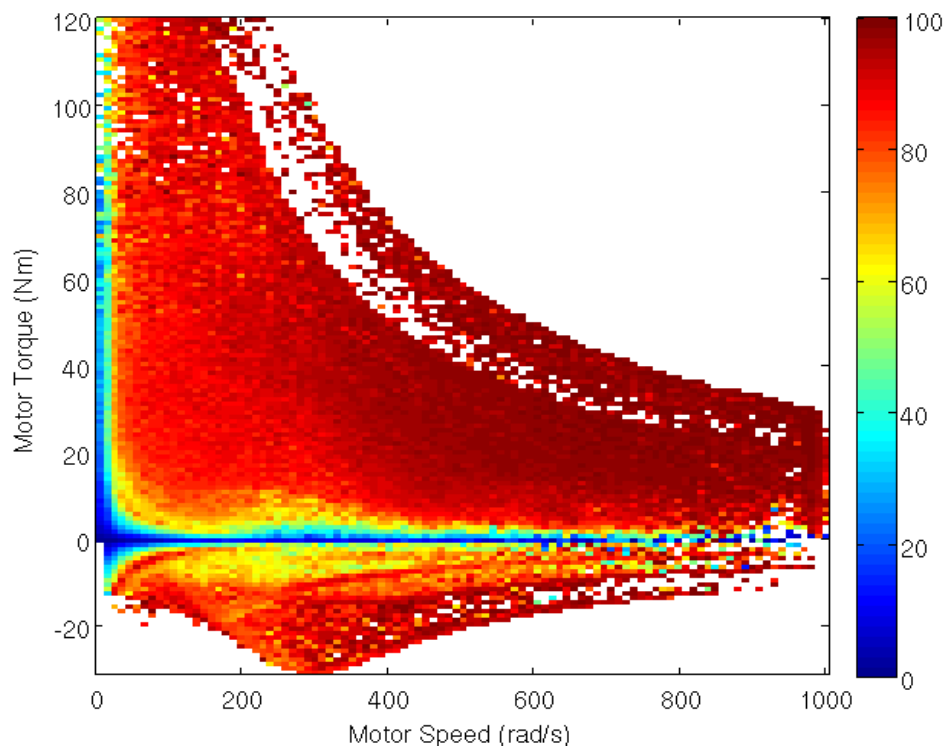
The first part of this subsection consists of the model execution equations (Stage 4). The Smart ED employs a 55 kW brushless DC machine. For the PHEV model, the electric machine and the associated inverter have been considered as a single integrated system. The final drive ratio (g_{fd}) is given as 8.67. As discussed in [13], the values of battery terminal voltage (v_t), battery current (i_b) and the rotational velocity of the machine (ω_{em}) were recorded under a number of different operating conditions during vehicle evaluation. These values were used within Equations (4–6) to calculate the efficiency of the electric drive system. Figure 3 shows the mean efficiency for the electrical machine expressed as a function of shaft torque (T_{em}) and rotor velocity for the baseline map of 30 kW. This map is loaded at Stage 1 of the simulation. Further information regarding the derivation of this figure is provided in [13]:

$$T_{em} = \frac{T_w}{g_{fd}} \quad (4)$$

$$\omega_{em} = \omega_w \cdot g_{fd} \quad (5)$$

$$\eta_{em} = \frac{T_{em} \cdot \omega_{em}}{v_t \cdot i_b} \quad (6)$$

Figure 3. Efficiency of electric machine (η_{em}).



In order to employ the model within the optimization study, Equation (7) shows how the torque (T_{em}) of the efficiency map can be scaled as a function of the peak power requirements of the subsystem ($P_{em(peak)}$). This equation is represented as EM scale function at Stage 2 of the simulation:

$$T_{em} = T_{em(base)} \cdot \frac{P_{em(peak)}}{30,000} \quad (7)$$

where 30 kW is the maximum power of the conventional Smart ED machine. This approach has been successfully applied in a number of comparable optimization studies reported in the literature [10,16]. When scaling the torque and efficiency characteristics of the electrical machine, the same regenerative braking strategy observed from Figure 3 is maintained. Finally, using manufacturers published data, the mass of the electrical machine and inverter system is updated using a linear function of peak power (g_{em}) [17]:

$$M_{em} = g_{em}(P_{em(peak)}) \quad (8)$$

3.3. Battery Model

Within the HV battery model during model execution, SoC is quantified using the generic method of coulomb counting, in which SoC_{init} defines the initial condition of the battery SoC and Q_b the capacity of the battery expressed in Ah:

$$SoC(t) = \frac{SoC_{init} \cdot Q_b \cdot 3,600 - \int_0^t i_b \cdot dt}{Q_b \cdot 3,600} \quad (9)$$

In order to ascertain the real-world operating efficiency of the HV battery a Rint type equivalent circuit model was used. This method is widely reported within the literature and comprises of an open circuit voltage (v_{oc}) in series with a charge and discharge resistance (R_b) [18]. The value of v_{oc} was estimated using the data recorded from [13]. The data was analyzed and the points in which i_b was zero were noted. Under these conditions, the value of v_{oc} equals the measured battery terminal voltage (v_t). Figure 4 shows the result of this exercise and presents the estimated value of v_{oc} as a function of measured battery temperature and SoC. This map is loaded at Stage 1 of the simulation. Further information regarding the derivation of this Figure is provided in [13]. For a given value of i_b , the battery terminal voltage can be calculated using Equation (10):

$$v_t = v_{oc} - i_b \cdot R_b \quad (10)$$

In order to calculate i_b and v_t , battery power is calculated based on Equation (11). P_{aux} is the auxiliary power needed for the vehicle and includes such loads as the headlights, air conditioning, entertainment system *etc.* On average this was measured at 1kW within the Smart ED. P_{em} is the power of the electric machine and is equal to the drive power demand. Within a PHEV, the energy management strategy must control the engine power (P_{ice}) to ensure that the power constraints and SoC of the battery are not exceeded:

$$P_b = P_{em} + P_{aux} - P_{ice} \quad (11)$$

As part of the optimization routine discussed in Section 5.1, Equations (12–15) present how the HV battery is *scaled* by altering the number of parallel strings (n_p). This set of equations is executed at Stage 2 of the simulation as the battery function to create the v_{oc} map. The number of cells in series (n_s) is maintained constant to ensure compatibility with the electrical machine:

$$R_b = R_{cell} \cdot \frac{n_s}{n_p} \quad (12)$$

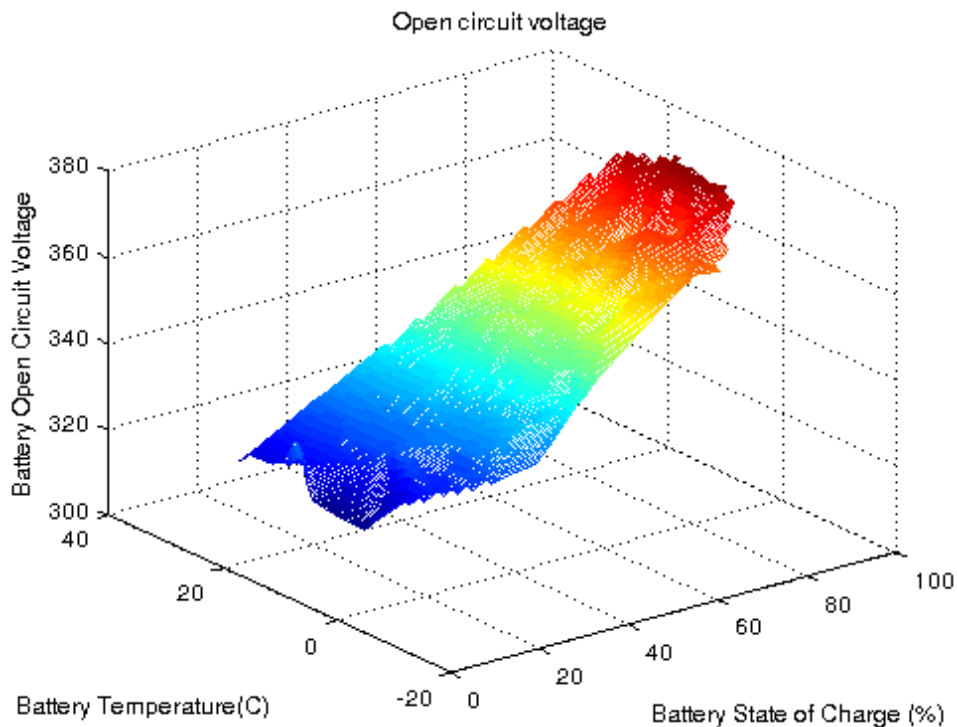
$$V_{oc} = V_{oc(cell)} \cdot n_s \quad (13)$$

$$Q_b = Q_{cell} \cdot np \quad (14)$$

$$M_b = M_{cell} \cdot np \quad (15)$$

It is noteworthy that the mass of each cell (M_{cell}) includes not just the cell mass but also a weighting term to account for the mass compounding effects of introducing large battery systems.

Figure 4. Measured battery open circuit voltage.



3.4. Integrated ICE and Generator

The ICE model consists of two parts. In the first part a scalable fuel consumption map is developed. This part is represented as the ICE function in Stage 1 of the simulation. In the latter part the derived scalable map is combined with the electric machine map to give a combined efficiency map. This map is used to identify the best specific fuel consumption line (BSFC) of the engine. These steps are carried out at Stage 2 of the model execution. The BSFC line is then used in the simulation model to calculate fuel consumption.

3.4.1. Creation of Engine Efficiency and Fuel Consumption Map

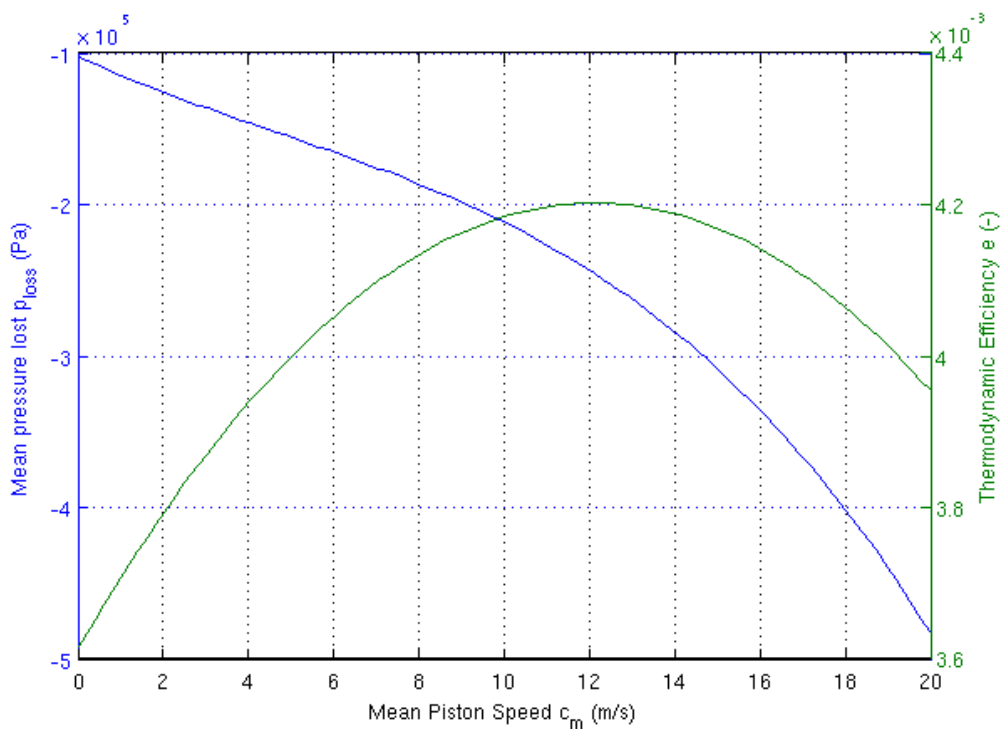
Creation of the scalable ICE model was first proposed in [19] by using the Willans line technique. Later the methodology was improved and used to size the ICE components of a HEV in [20]. The concept is based on the average pressures acting on top of an imaginary piston to produce the same torque as the ICE. Consider the expression shown in Equation (16), p_{mf} is the ideal pressure acting on top of the piston in the case of no losses and all chemical energy being converted to mechanical energy. The term e , can be described as the thermodynamic efficiency of the engine and p_{loss} is the pressure loss due to the mechanical losses in the system. The resulting average pressure p_{me} is the mean effective pressure which is equivalent to the engine producing torque T_e . The peak value of p_{me} is

fixed for a type of engine and is expressed as a function of the mean piston speed c_m . p_{loss} and e can also be defined as functions of c_m . The value of these terms does not change for different engine volumetric sizes for a particular engine technology, which has been validated in [19].

A map of these three parameters was obtained from [19] for a naturally aspirated three cylinder engine. The variation of these parameters with c_m is shown in Figure 5. This base map is loaded in Stage 2 of the simulation. The experimental work performed in [19] shows that e can also be expressed by c_m and p_{mf} to capture the reduction in efficiency of the system during high load conditions:

$$p_{mf} = \frac{p_{me} + p_{loss}}{e} \tag{16}$$

Figure 5. Estimated p_{loss} and e of engine.



From the value of p_{mf} the fuel flow rate can be calculated based on Equation (17), where H_l is the lower heating value of fuel and V_d is the volumetric size of the engine:

$$\dot{m}_f = \frac{p_{mf} \cdot V_d}{H_l} \tag{17}$$

Finally in order to convert the p_{me} values to engine torque T_e and c_m values to engine speed Equations (18–19) are used:

$$T_e = \frac{p_{me} \cdot V_d}{N_{cyl} \cdot \pi} \tag{18}$$

$$\omega_e = \frac{c_m \cdot \pi}{S} \tag{19}$$

N_{cyl} represents the number of power strokes per cycle. In this case it is 4 since the engine is a 4-stroke engine. S represents the stroke length of the engine, based on the original data 0.067 m was

used. As a result, a fuel consumption map with engine speed and engine torque as the *x*- and *y*-axis has been developed for a particular volumetric size which is shown in Figure 6.

In order to perform an initial validation of the derived ICE efficiency map, the baseline model was incorporated with the vehicle model [Equations (1) and (2)] and then exercised over the NEDC in a backward facing simulation. The fuel consumption was found to be 5.49 L/100 km. manufacturer’s published data for the vehicle cites a value of 5.64 L/100 km, 2% greater than the estimated value.

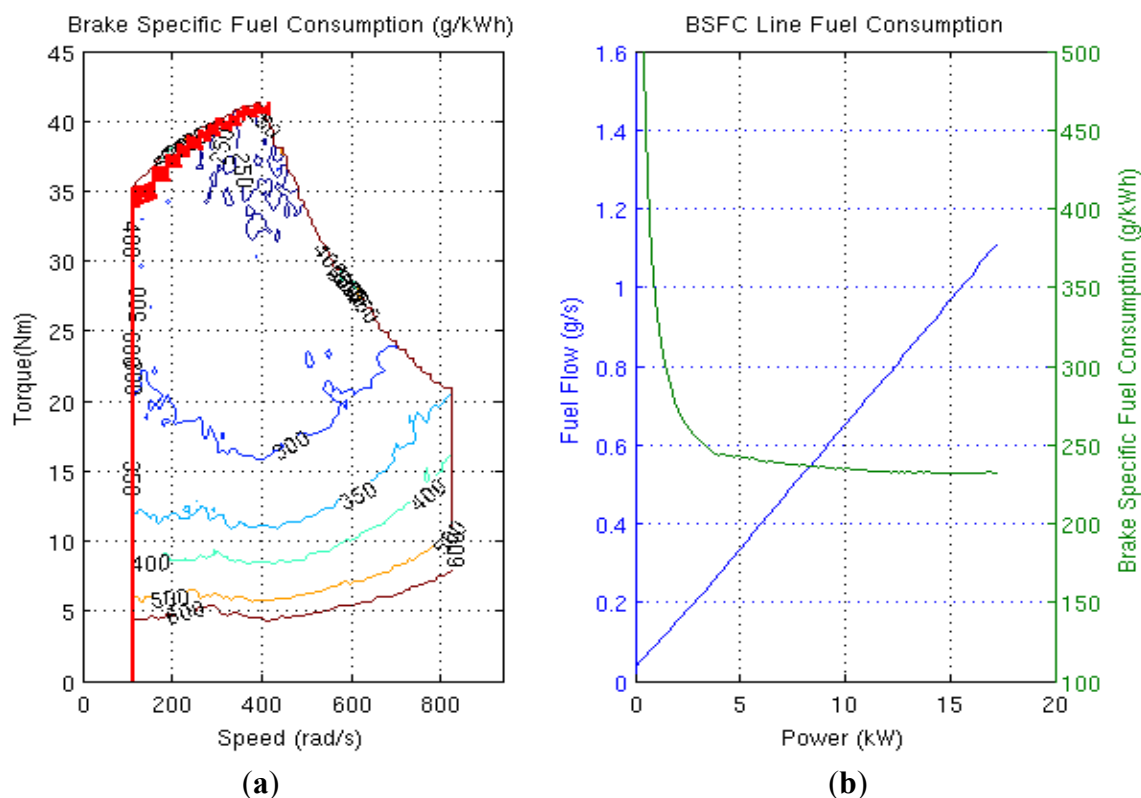
3.4.2. Identification of best operating line

In the second part, the map of an electric machine is formulated using the scaling procedure described in Section 3.2. The peak power of the machine is matched such that the electric machine has enough power to work across the entire BSFC line. In order to identify the BSFC line the fuel consumption map is converted to an efficiency map of the engine and combined with the electric machine efficiency. The equation to convert fuel consumption to engine efficiency is given below:

$$\eta_e = \frac{T_e \cdot \omega_e}{m_f \cdot H_l} \tag{20}$$

For each power point, the combination of speed and torque values which give the highest efficiency is identified. Finally for the best operating speed, torque points corresponding fuel consumption is determined from the previously derived map. The fuel consumption map and the best operating points for a 0.5 L ICEis shown in Figure 6.

Figure 6. Operating line for best specific fuel consumption. (a) Based on torque-speed map; (b) Power-fuel-flow line.



3.5. Financial Cost Model

Several financial cost metrics have been proposed within the literature to quantify and evaluate different technology options within the automotive sector. As discussed in [16,21], these include the procurement cost of components, their operating cost and the residual cost or value that may be realized at the vehicle end of life (EOL). The primary aim of this research is to quantify the financial cost of powertrain components installed within the PHEV at the point of sale to the consumer. Research published by the National Renewable Energy Laboratory (NREL) in [22,23] quantifies system cost for the HV battery, electrical machine and ICE.

Equation (21) defines the installed cost of the battery pack as a function of peak power (P_b) and energy (E_b). Conversely, Equations (22) and (23) define the financial cost of both the electrical machine and the ICE as a function of their respective peak power requirements. A full derivation of the financial weightings are discussed in [23] and will therefore not be repeated here. However, it is noteworthy that the authors include factors such as market segmentation, vehicle class, and the expected profitability within their analysis. Validation of the empirical relationships is provided, where the authors verify the financial cost equations for existing commercially available EVs and HEVs:

$$\text{Battery Cost} = \$22 \cdot P_{b(\max)} + \$700 \cdot E_b + \$680.00 \quad (21)$$

$$\text{Motor Cost} = \$21.70 \cdot P_{em(\text{peak})} + \$480.00 \quad (22)$$

$$\text{Engine Cost} = \$14.50 \cdot P_{ice(\text{peak})} + \$531.00 \quad (23)$$

4. Energy Management Control Strategy

4.1. Thermostat/Heuristic Rule-based Control Strategy

When the vehicle is operating in a CS mode using a heuristics or rule-based control strategy, the main objective is to maintain the SoC of the HV battery within a lower and upper threshold. Traditionally, the control strategy is presented as either combinatorial logic or a state transition diagram [19]. Algorithm 1 presents the pseudo code for the thermostat energy management strategy employed within this study. As it can be seen, the control system will activate or deactivate the ICE to maintain the HV battery within a lower and upper SoC region. In addition, the power demand sent to the ICE (P_{ice}) is modified to ensure that the HV battery limits are not exceeded during charging.

For the purpose of this study, the UPPER THRESHOLD calibration has been optimized for each drivecycle under investigation. Within [11], consideration is given to the sensitivity of a rule-based approach for variations in the power demand of the drivecycle. For reference, Figure 7 presents the simulated performance of a PHEV over the NEDC for different calibrations of the upper threshold. For each simulation, the lower threshold was set to 25% SoC. As it can be seen, the energy consumption and resultant CO₂ emissions are variable and largely dependent on the magnitude of the residual energy within the battery at the end of the cycle. An energy value above 25% SoC ultimately relates to electrical energy that has not been employed to propel the vehicle. Furthermore, the source of this energy will have come in part from the ICE and therefore the burning of fossil fuels.

Algorithm 1. Pseudo code for the thermostate energy management control strategy.

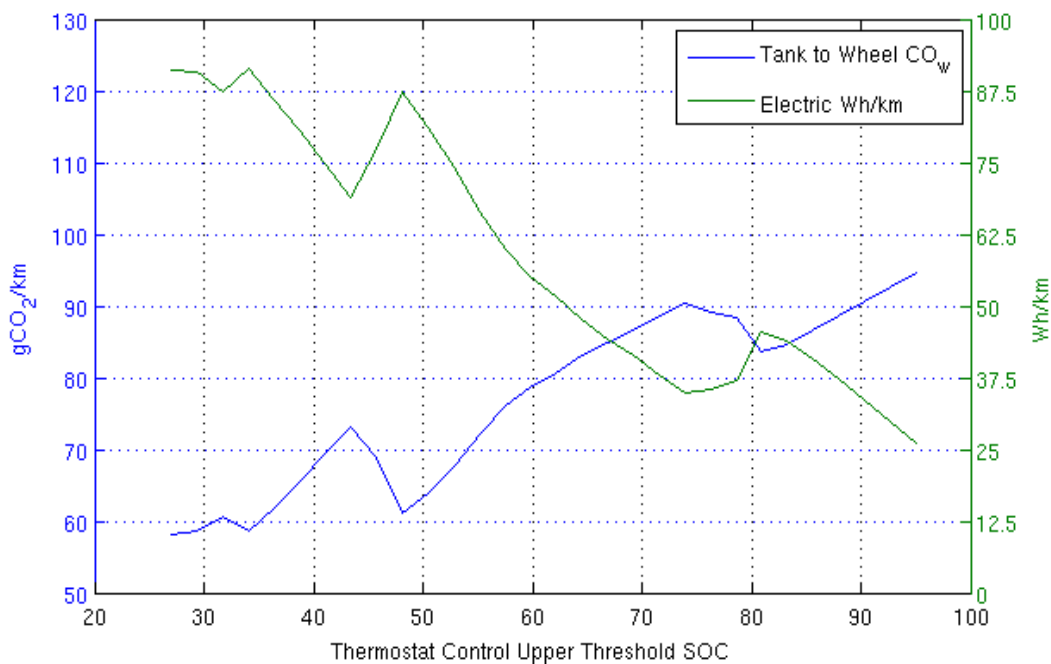
```

if (SoC < LOWER TRESHOLD)
    Engine is switched on
else if (SoC > UPPER THRESHOLD)
    Engine is switched off
else if (P_dmd > P_bat(max))
    Engine is switched on
else
    Repeat previous state
end

if (P_eng_best > P_bat + P_dmd)
    P_eng = P_bat + P_dmd
else if (P_eng_best < P_dmd - P_bat)
    P_eng = P_dmd - P_bat
else
    P_eng = P-eng_best
end

```

Figure 7. Influence of upper threshold.



4.2. Improved Equivalent Consumption Minimization Strategy (ECMS)

The ECMS of local cost function optimization was first proposed by [24] for a HEV and later refined and extended within a number of research publications [9,25–28]. For a given value of driver demand power P_{dmd} , optimization of the energy consumption within the PHEV is achieved by selecting the optimal instantaneous power split (β) between the ICE (P_{ICE}) and HV battery (P_B) while adhering to the minimum and maximum power constraints within the PHEV:

$$P_{ICE} = \beta \cdot P_{dmd} \quad (24)$$

$$P_B = (1 - \beta) \cdot P_{dmd} \tag{25}$$

$$P_{ICE_MIN} \leq P_{ICE} \leq P_{ICE_MAX} \tag{26}$$

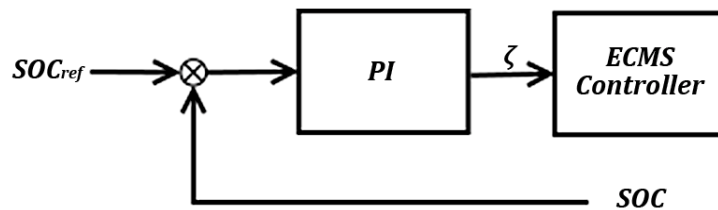
$$P_{B_MIN} \leq P_B \leq P_{B_MAX} \tag{27}$$

The locally optimized value of β that provides the most efficient power split between the ICE and electrical machine is calculated at each time-step, by minimizing the cost function (J):

$$J = MIN(g + g_{equiv} \cdot \zeta) \tag{28}$$

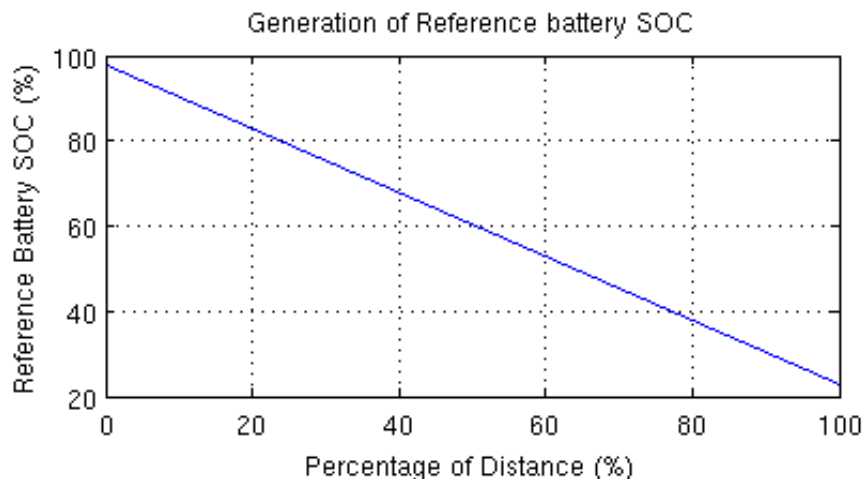
The term g represents the instantaneous mass flow rate of fuel from the ICE and g_{equiv} represents the equivalent amount of fuel used by the battery to deliver P_B . Finally ζ defines the charge-sustaining penalty function. The value of ζ is calculated from an outer proportional plus integral (PI) control loop. The output from the integral term of the controller is saturated between the values of 0 and 10 in order to avoid potential instability through the occurrence of integral windup. However, it is noteworthy that for the drivecycles evaluated the controller limits were never exceeded. Figure 8 presents the structure of the improved ECMS control system. Further information regarding the design and parameterization of this control system and the energy consumption improvements associated with its use are discussed in [11].

Figure 8. Improved PI–ECMS energy management approach.



As discussed in [11] for the controller to operate as a CB energy management strategy, a SoC trajectory (SOC_{ref}) must be defined and known in advance by the control system. For this research, an approximation is made based on the work undertaken in [11]. Figure 9 presents the reference trajectory, in which SoC is a linear function of journey distance.

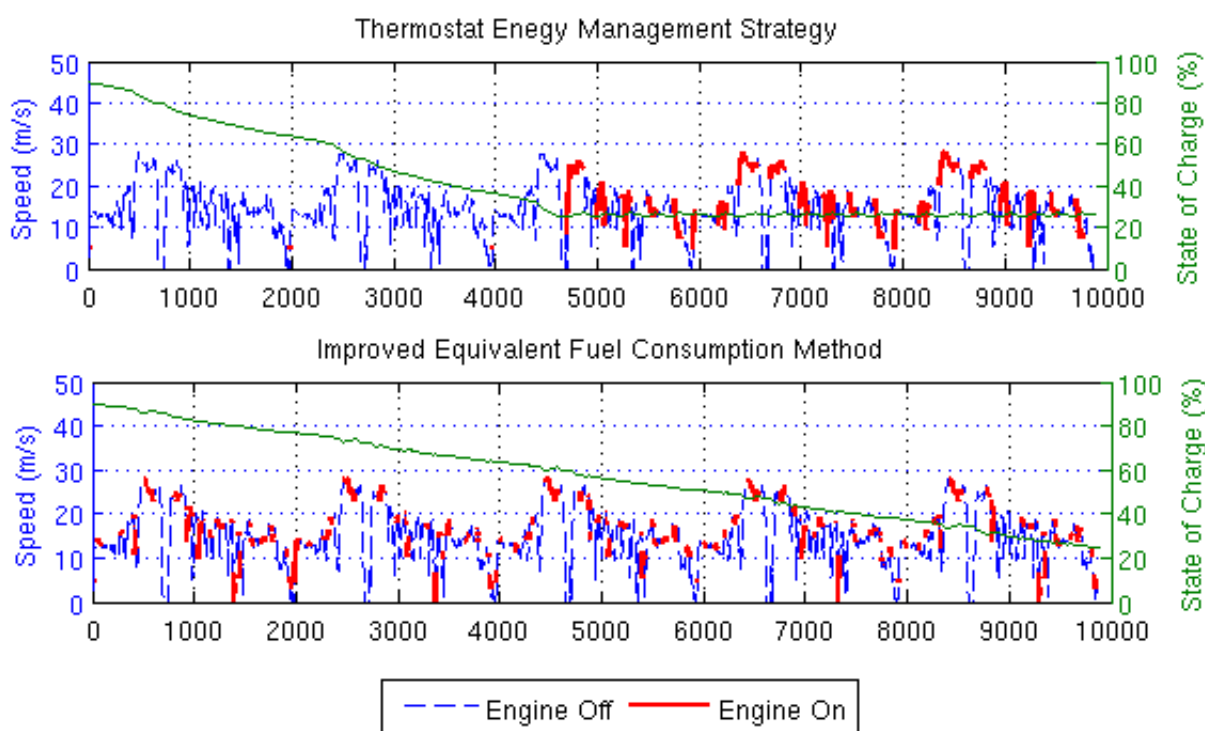
Figure 9. Reference battery SOC.



4.3. Control System Comparison

A critical review of the comparison between a thermostat strategy, in which the vehicle operates in a CD and CS mode and a PHEV operating in CB mode using the advanced ECMS is presented in [11]. For illustration purposes, Figure 10 presents an example set of results in which the model of the PHEV is exercised over a real-world drivecycle recorded as part of the EV evaluation programme. For the CB energy management approach, reductions of 3% to 7% in tank-to-wheel CO₂ emission can be realized. As discussed in previous studies [10], the primary reason for the improved energy efficiency, is that the ICE is able to operate in a higher efficiency region for comparatively longer during the trip.

Figure 10. Engine ON/OFF events for different control strategies.



5. Component Sizing

5.1. The Optimization Algorithm

The optimization algorithm employed as part of this study is codified within Matlab as the function; *fminsearch* and represents a derivative-free local optimization routine. For a given set of initial conditions, the optimizer makes use of a *neighborhood* search method to identify the local optimal solution. From a review of existing literature, this algorithm has not been previously employed for optimizing the powertrain components within a PHEV. However, within the broader context of automotive design, the algorithm has been successfully used for parameter estimation to predict capacity degradation within a battery [29] and for identifying the optimal transmission ratios within a hydraulic hybrid vehicle [30].

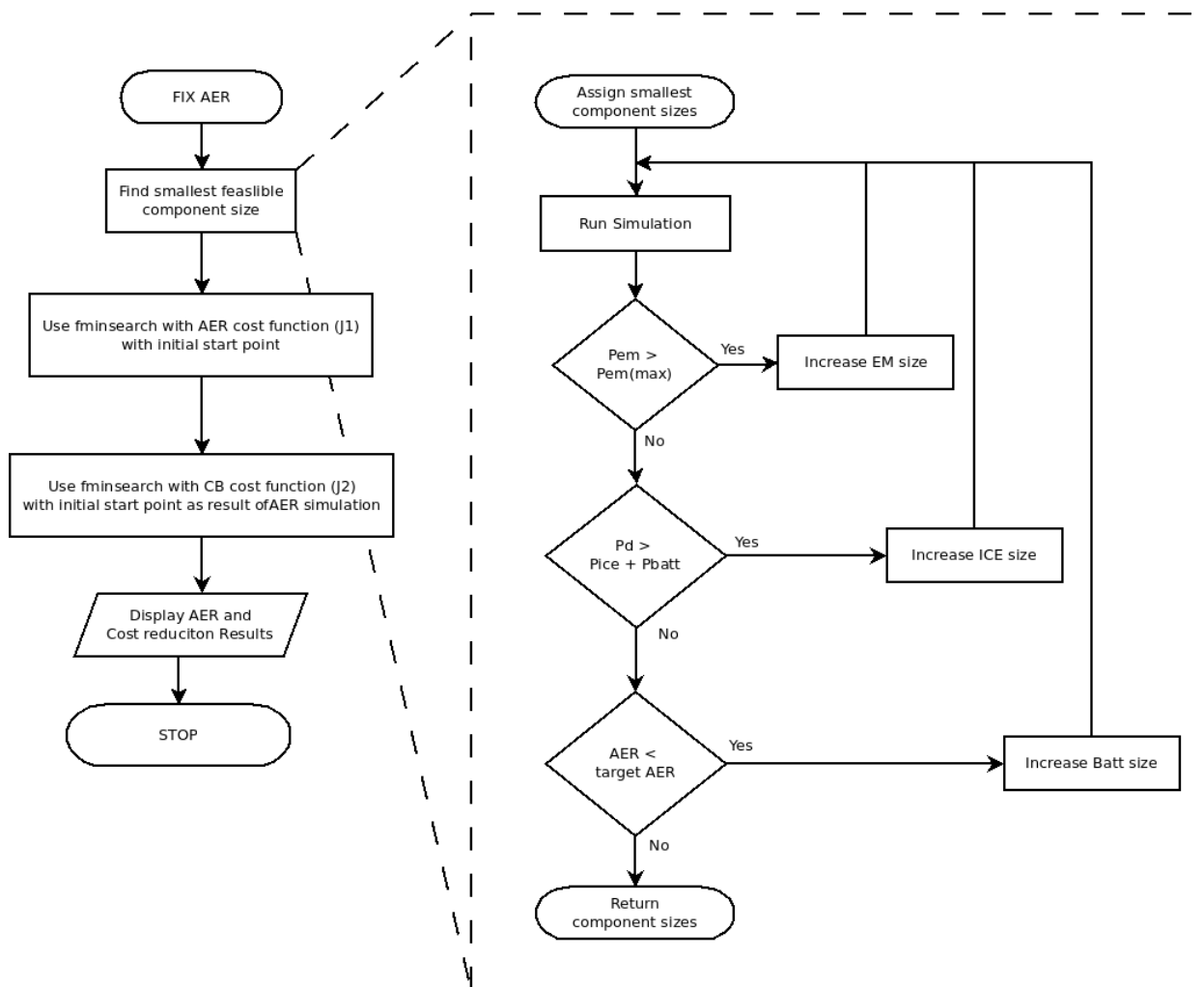
A full description of the optimization routine underpinning *fminsearch* and the method for detecting convergence is provided in [31]. The optimization method employs the Nelder–Mead simplex

algorithm. A simplex is defined as a set of $n + 1$ points, where n represents the number of parameters to be optimized. For example, in the case where $n = 2$, the simplex forms a triangle *around* the initial solution. For a given cost function, the optimization routine evaluates each point on the simplex to identify if it represents a better performing solution. If one is found, then a new simplex is created around that individual. Convergence is reached, when the size of the simplex has been sufficiently reduced and a better performing individual cannot be identified within the local search space [31].

5.2. The Optimization Framework

As shown in Figure 11, in order to quantify the component downsizing opportunities associated with the use of a CB energy management approach within a PHEV, a three stage optimization process has been employed.

Figure 11. Overall component sizing procedure.



Firstly, for a given AER and drivecycle, the PHEV model developed in Section 3, is executed within an iterative loop. Initial conditions for the energy capacity of the HV battery, the peak power rating of the electrical machine and volumetric size of the ICE are defined as; 9 kWh, 10 kW and 0.5 L respectively. For each execution of the model, if a component constraint is exceeded, the simulation terminates and then restarts with an increased component size. If the PHEV is able to meet the power

requirements of the drivecycle, and the HV battery is depleted to the lower threshold, the simulation terminates and the parameterization set for the powertrain is deemed to represent the smallest feasible set of components for that drivecycle and target AER. For this initial simulation the upper threshold of the thermostat strategy is fixed at 30% SoC. It is noteworthy that a similar approach is adopted within the commercially available PSAT simulation environment for the sizing of EV and HEV powertrain components.

The optimization algorithm within Stage 2 solves the cost function (J_2), defined in Equation (29). The inputs to the optimization process are:

- Engine volumetric size (V_d);
- Electric machine power ($P_{em(peak)}$);
- Battery number of strings in parallel (np);
- Upper threshold calibration for the thermostat controller.

The results from Stage 1 provide the initial conditions for each of the above parameters. For each iteration of the optimizer, the PHEV model derived in Section 3 is executed to ascertain the vehicle’s AER and CO₂ emissions. These values are then weighted by $fn1$ and $fn2$ within J_2 . Plots of the parabolic functions are presented in Figure 12. The weighting of the two parameters of the cost function were calibrated such that the optimization returned the desired AER. The constraints during the simulation are given by Equations (30–32). If any of the constraints are violated an artificially high number is returned to the optimizer to deem the set of inputs as infeasible. For the final set of PHEV powertrain components, Equations (21–23) were used to calculate the financial cost of the powertrain:

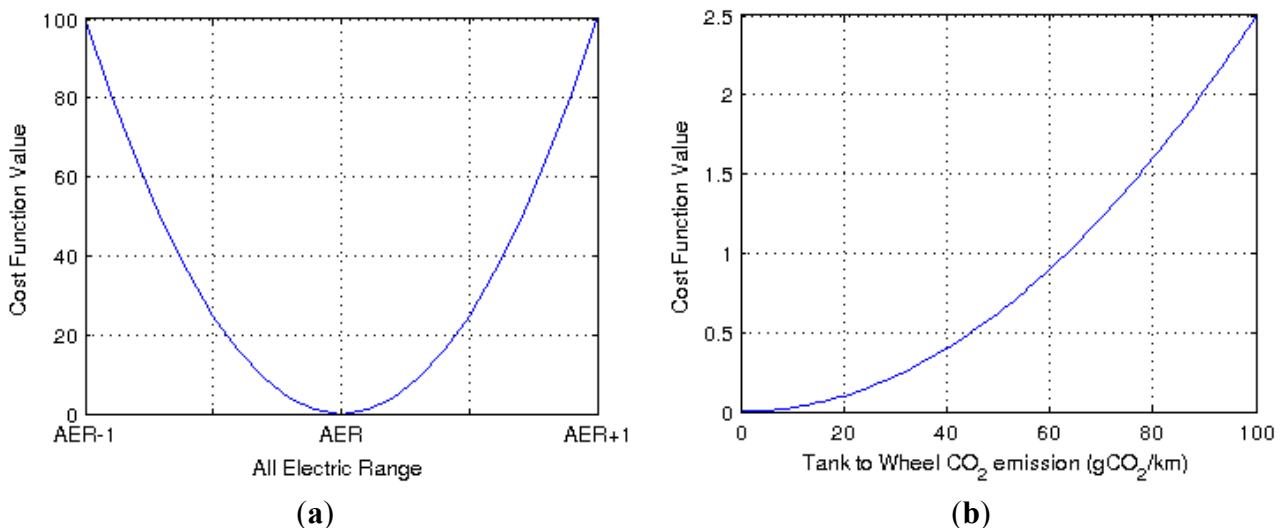
$$J_2 = MIN(fn1(AER) + fn2(CO_2)) \tag{29}$$

$$0 \leq P_{ice} \leq P_{ice(peak)} \tag{30}$$

$$T_{em} \leq T_{em(scaled)} \tag{31}$$

$$P_{b(min)} \leq P_b \leq P_{b(max)} \tag{32}$$

Figure 12. Cost function for thermostat based PHEV. (a) Parabolic equation $fn1$; (b) Parabolic equation $fn2$.



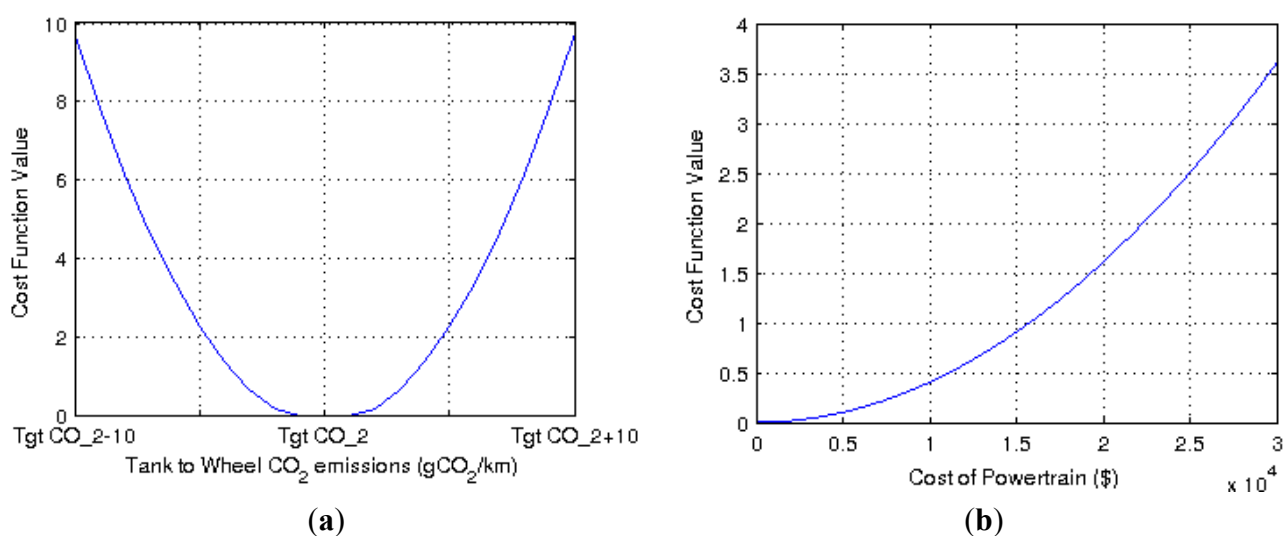
For a given drivecycle and target AER, the output from Stage 2, is a re-optimized set of PHEV powertrain components, including the upper threshold calibration for the thermostat strategy. When comparing the results from Stage 1 and Stage 2, it is noteworthy that the optimized set of PHEV powertrain components does not necessarily equate to the smallest feasible component sizes. It has been observed for example, that the optimization routine may return a larger electrical machine, so as to facilitate greater levels of regenerative braking during the drivecycle.

For the same drivecycle and AER, the final stage (Stage 3) of the optimization framework is to quantify if further PHEV component downsizing can be realized through the use of a CB energy management strategy. The optimization routine is seeded using the resultant values from Stage 2. Once again, for each data-set of engine volumetric size, number of parallel strings and electric machine peak power, the PHEV model is executed with the improved ECMS approach. The same constraints are applied as Stage 2. With the CB approach, Figure 9 defines the target SoC profile across the drivecycle. The ECMS defines the instantaneous optimal power split between the ICE and the HV battery. For each PHEV solution, the resultant CO₂ emissions and the financial cost of the hybrid powertrain are calculated, using Equations (21–23). In order to solve J_3 , the weighting functions $fn3$ and $fn4$ are applied within the cost function J_3 :

$$J_3 = \text{MIN}(fn3(\text{CO}_2) + fn4(\text{Cost})) \quad (33)$$

The constraints applied to the optimization are as previously defined by Equations (30–32). A plot of the parabolic functions, $fn3$ and $fn4$, are presented in Figure 13. The relatively high weighting of $fn3$, ensures that the required target CO₂ values are achieved, thereby facilitating an equitable cost comparison to be made between those PHEV solutions that employ the traditional thermostat strategy and those that have been re-optimized using the improved ECMS approach to energy management.

Figure 13. Cost function for charge blended PHEV (a) Parabolic equation $fn3$; (b) Parabolic equation $fn4$.



6. Results

6.1. PHEV Powertrain Cost Reduction

Figure 14 presents the total cost of the PHEV powertrain for the different CO₂ thresholds corresponding to the AERs of 48, 64, 80 and 96 km (30, 40, 50 and 60 miles). As it can be seen, the financial cost of the powertrain increases as the aggressiveness of the drivecycle increases. Inline with [32] within the context of this research, aggressiveness relates to the levels of vehicle acceleration and braking experienced within the drivecycle. For the same energy management strategy, the PHEV powertrain cost can increase by as much as 15% when comparing the two solutions; one optimized for the NEDC and the other optimized for the more aggressive, Artemis cycle. In all instances as the required AER for the PHEV increases so does the financial cost of the powertrain. For twice the AER the financial cost of the powertrain increases by a factor of 1.5. Furthermore, Figure 15 clearly shows that the HV battery system dominates the financial cost of the hybrid powertrain.

Figure 14. Cost comparison among different options.

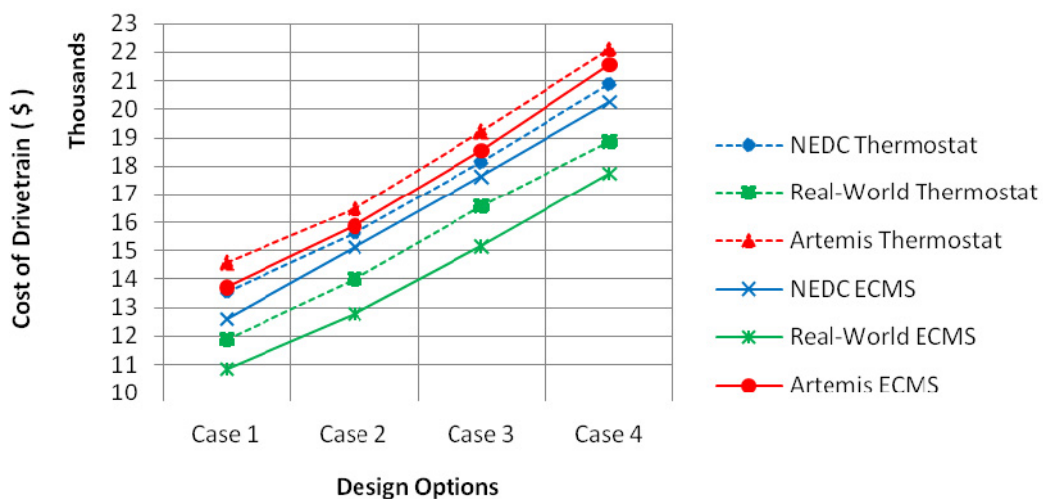
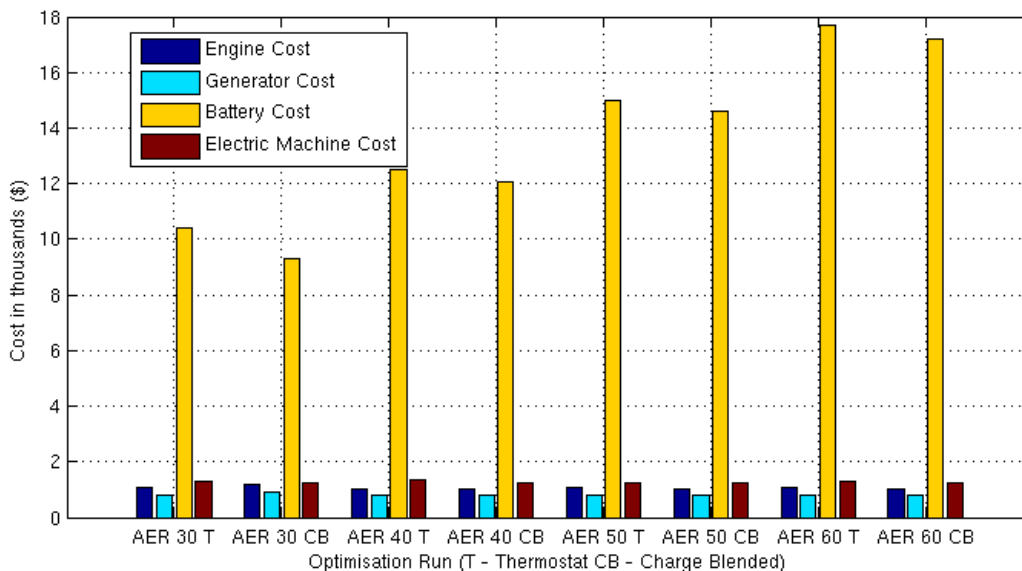


Figure 15. Component cost for different NEDC optimization runs.



When comparing the impact of the energy management strategy on the financial cost of the powertrain, Figure 14 highlights that optimization of the powertrain using the improved ECMS, consistently delivers cost reductions in the order of 3%–7%. Table 2 quantifies the financial cost reductions that may be achieved at the component level.

6.2. Downsizing of the HV Battery

Figures 16 and 17, present the downsizing opportunities within the HV battery both in terms of energy capacity and power capacity. Given the dominant cost of the HV battery system, there is a high degree of correlation between Figures 14, 16 and 17. When considering the different drivecycles; (NEDC, Artemis and Real-World) for design Case 2 and CO₂ thresholds of 55, 71 and 77 g CO₂/km the size of the HV battery system may be reduced by up to 3.7%, 4% and 10% respectively. The reduced requirement for energy storage onboard the vehicle, stems directly from the improved ECMS philosophy and the optimal use of both the ICE and the battery for the duration of the journey.

Figure 16. Battery energy for different options.

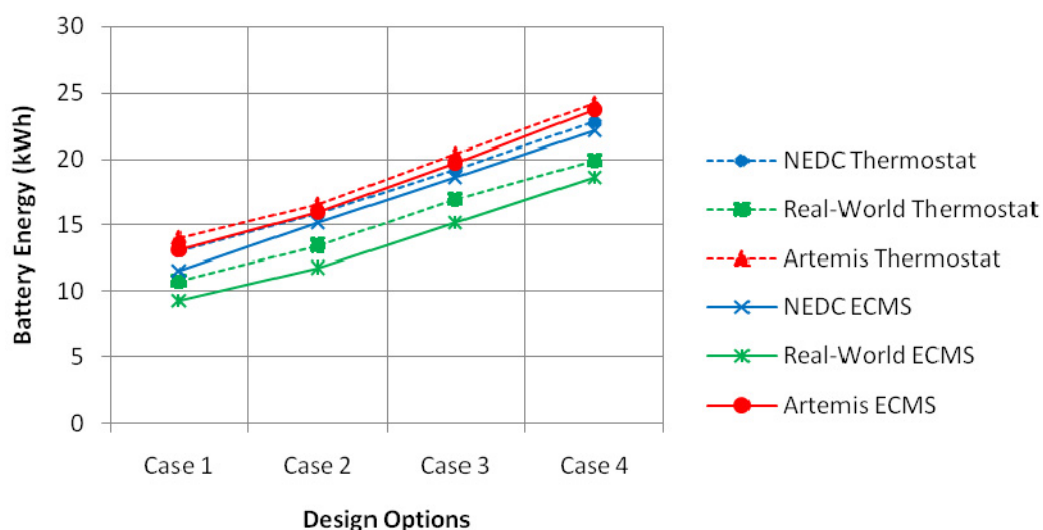


Figure 17. Battery power for different options.

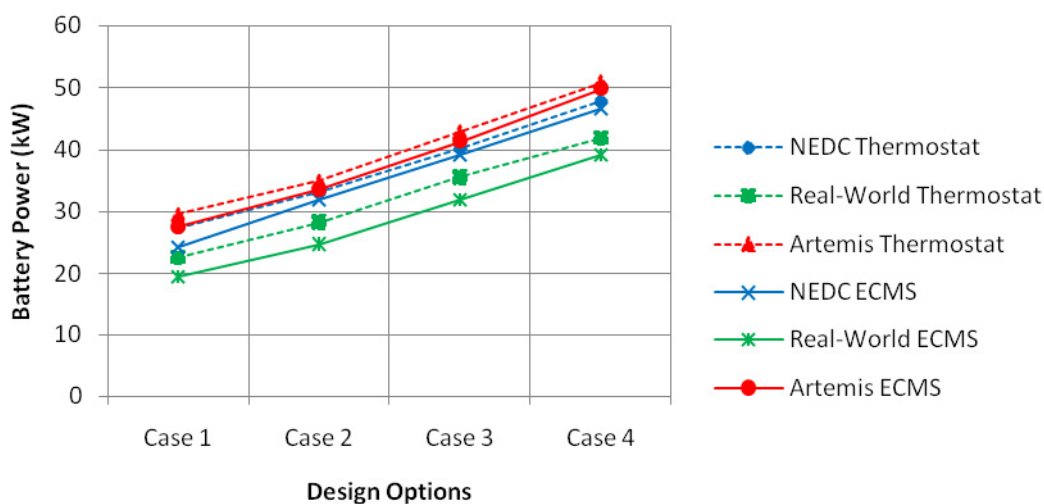


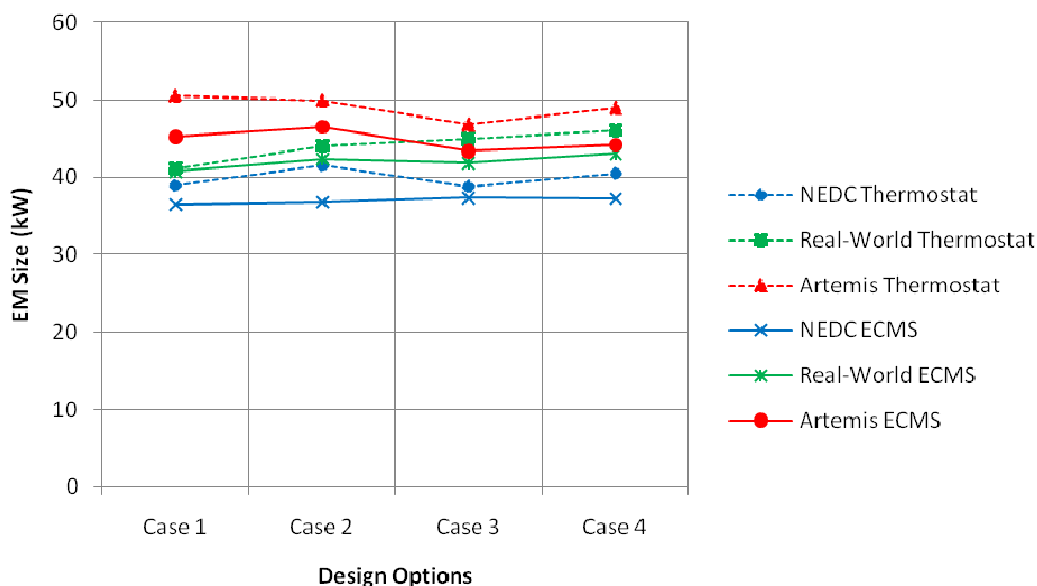
Table 2. Results of component sizing.

Drivecycle: NEDC												
Parameters	Design Case 1			Design Case 2			Design Case 3			Design Case 4		
	Thermostat	Improved ECMS	Change									
AER (km)	48			64			80			96		
Vd (mL)	538.13	650.28	21%	507.82	531.90	5%	541.43	500.06	−8%	537.36	500.01	−7%
Pice (kW)	18.02	21.54	20%	16.98	17.79	5%	18.14	16.75	−8%	17.99	16.75	−7%
Pem (kW)	38.95	36.50	−6%	41.52	36.80	−11%	38.88	37.35	−4%	40.49	37.30	−8%
Pbat (kW)	27.32	24.33	−11%	33.21	31.95	−4%	40.19	39.12	−3%	47.88	46.51	−3%
Qbat (kWh)	13.02	11.59	−11%	15.82	15.22	−4%	19.15	18.64	−3%	22.81	22.16	−3%
TTW (g CO ₂ /km)	69.99	70.51	1%	54.68	55.26	1%	39.62	40.12	1%	23.29	23.61	1%
Cost (\$)	13,538.67	12,607.44	−7%	15,635.85	15,126.79	−3%	18,118.63	17,633.27	−3%	20,877.84	20,260.40	−3%
Drivecycle: Real-World												
Parameters	Design Case 1			Design Case 2			Design Case 3			Design Case 4		
	Thermostat	Improved ECMS	Change									
AER (km)	48			64			80			96		
Vd (mL)	528.00	562.91	7%	546.26	584.83	7%	532.27	500.57	−6%	554.58	500.42	−10%
Pice (kW)	17.65	18.66	6%	18.32	19.39	6%	17.81	16.77	−6%	18.44	16.76	−9%
Pem (kW)	41.17	40.74	−1%	44.05	42.35	−4%	44.95	41.82	−7%	46.06	43.05	−7%
Pbat (kW)	22.60	19.53	−14%	28.24	24.75	−12%	35.53	31.84	−10%	41.77	39.08	−6%
Qbat (kWh)	10.77	9.30	−14%	13.46	11.79	−12%	16.93	15.17	−10%	19.90	18.62	−6%
TTW (g CO ₂ /km)	83.17	83.61	1%	77.23	77.82	1%	68.40	68.98	1%	59.97	60.55	1%
Cost (\$)	11,890.76	10,846.26	−9%	13,990.67	12,776.07	−9%	16,578.49	15,143.13	−9%	18,856.06	17,744.06	−6%
Drivecycle: Artemis												
Parameters	Design Case 1			Design Case 2			Design Case 3			Design Case 4		
	Thermostat	Improved ECMS	Change									
AER (km)	48			64			80			96		
Vd (mL)	534.05	500.02	−6%	553.96	501.71	−9%	539.05	501.35	−7%	545.27	500.12	−8%
Pice (kW)	17.87	16.75	−6%	18.49	16.81	−9%	18.06	16.79	−7%	18.28	16.75	−8%
Pem (kW)	50.59	45.24	−11%	50.00	46.58	−7%	46.77	43.39	−7%	48.94	44.25	−10%
Pbat (kW)	29.52	27.62	−6%	34.87	33.57	−4%	42.79	41.33	−3%	50.81	49.77	−2%
Qbat (kWh)	14.07	13.16	−6%	16.61	15.99	−4%	20.39	19.69	−3%	24.21	23.71	−2%
TTW (g CO ₂ /km)	81.98	83.37	2%	71.48	72.99	2%	57.60	59.17	3%	43.54	45.10	4%
Cost (\$)	14,565.78	13,716.97	−6%	16,486.78	15,863.46	−4%	19,210.74	18,554.40	−3%	22,117.47	21,570.86	−2%

6.3. Optimization of the Electrical Machine and ICE

Figure 18 presents a reduction in the power requirements of the electrical machine through the use of CB energy management strategy. With respect to Table 2 for a given drivecycle and CO₂ threshold, reductions in the order of 3% to 7% may be realized.

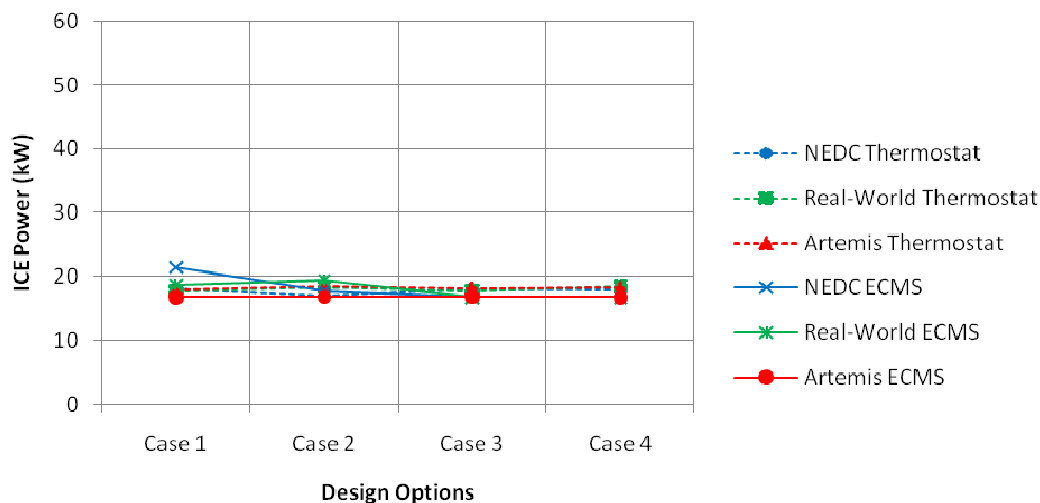
Figure 18. Variation of EM Power for different options.



As a result of the optimization, it is noteworthy that the peak power requirement of the electrical machine may not necessarily be the same as the HV battery. When both the ICE and the battery are delivering power to the wheels, the ICE can assist the battery during periods of high power demand. If the PHEV employs a thermostat control strategy, this can only occur when the vehicle is operating in a CS mode. However, within a CB approach the ICE is continually able to augment the power demands placed on the electrical subsystems.

With respect to regenerative braking, depending upon the aggressiveness of the drivecycle, it has been observed that the optimization framework may select an electrical machine with a larger peak power rating. Under these conditions the potential to recapture energy under vehicle braking outweighs the relative disadvantages associated with a larger and heavier electrical machine.

For a volumetric capacity of 0.5 L, the optimization framework continually limits the size of the ICE to a smaller value as possible. Across the different drivecycles and design options only a marginal increase in the ICE is suggested by the optimizer. Figure 19 shows the constant value of ICE power across the different design cases.

Figure 19. Variation of ICE Power for different options.

7. Discussion

7.1. PHEV Model

As discussed in [13], parameterization of the electrical components within the PHEV model was done using data experimentally obtained from a fleet of EVs operating in the real-world. One of the main limitations associated with the data-set is the restricted temperature range over which data was recorded. Since it has been widely reported in the literature [33], that extremes of temperature can decrease battery efficiency and reduce available capacity it is likely that such environmental conditions will impact the result obtained from the optimization framework. However, the author's assertion is that the underlying trend would be the same as the results presented here.

Data for the scalable model of the ICE was obtained from previously published research [20]. While the results presented in [20] have been experimentally validated, engine technology has advanced in recent years [34]. As a result, if models of such systems were included within the optimization routine, then it is conceivable that the use of ICEs would be more efficient leading to further downsizing within the battery and electrical machine.

7.2. Energy Management Control System

Both the thermostat and the improved ECMS have been optimized to reduce the tail-pipe CO₂ emissions from the PHEV. As a result, the optimization framework penalizes the use of the ICE in favor of the HV battery and electrical machine. While this approach is in keeping with current European legislation, in which only tail-pipe emissions are cited when defining vehicle performance, it does not take into account the CO₂ emission from the electrical grid that are required to replenish the battery SoC [14]. For example, given the UK electrical grid mix, the published emission figure is 594 g CO₂/kWh [35].

In addition to the well-to-wheel emissions another factor that is not taken into account is the degradation of the HV battery. Research published by [36], highlight that battery degradation is a function of battery depth of discharge (DoD) and the transient load placed on the battery. The inclusion

of such factors within the improved ECMS cost function represents a valuable area of future research. In addition, the inclusion of EOL battery costs with the battery cost function may further refine the output of the cost function J_3 during PHEV component optimization.

With respect to the CB energy management approach, the assumption was made that the SoC trajectory was a linear function of journey distance. As discussed in [26] further improvements in PHEV efficiency could be realized if a more accurate profile of the SoC could be known priori. One area of future research would be to more accurately define the SoC trajectory using information such as road-type definitions, traffic congestions levels and driving style [5].

7.3. Optimization Framework and Component Scaling

The method of component scaling within the optimization framework employed within this study is widely accepted within the literature [8,16,20]. Many studies have provided experimental validation of the functions used. Within the optimization framework presented here, the primary consideration for component scaling was component mass as a function of the respective power requirements. The assumption was made that this relationship is linear. However, in practice the inclusion of secondary mass compounding effects and the use ancillary devices may well result in a non-linear relationship between component peak power and mass. The assertion is made that irrespective of the exact nature of the function, the validity of the optimization framework holds true. This is within the context of this research, to understand the methodology and the trends within the technology. Further research may wish to explore this relationship to a higher level of detail. In addition, consideration may also be given to other system attributes such as component volume, particularly with respect to the HV battery that may constitute a pertinent design constraint.

The financial cost equations presented in Equations (21–23) represent the installed cost of the main powertrain components. While the report highlights the underlying trend between the respective components, it is noteworthy that absolute values may vary between manufacturer and component technology.

8. Conclusions

Contained within this paper is an optimization study in which the use of a CB control strategy is used to reduce the financial cost of key PHEV powertrain components. An improved ECMS of energy management has been used to ascertain the optimal power split within the powertrain as the PHEV traverses a drivecycle. The design of this strategy is based on previously published research. In order to properly evaluate the downsizing opportunities, comparisons are made against PHEV designs that employ a traditional thermostat strategy, in which the component sizes and controller switching thresholds have been optimized to deliver a specific AER over a drivecycle. The results presented support those published in comparable studies which highlight that the CB approach facilitates a more energy efficient design of PHEV. For a target CO₂ value and drivecycle, the co-optimization of the PHEV components and the ECMS strategy has resulted in between 3% and 14% reductions in the energy and power requirements of the HV battery. Since the HV battery represents the single largest contributor to vehicle mass and powertrain cost, it is proposed that potential cost reductions in the order of 3%–9%, would further support the sustainable market introduction of this variant of low carbon vehicle.

Acknowledgements

The research presented within this paper is supported by the UK Technology Strategy Board (TSB) through the Knowledge Transfer Partnership (KTP) scheme in collaboration with the Morgan Motor Company.

Appendix

A1. Drivecycles

The drivecycles used in the simulation and optimization study are shown in Figures A1–A3. An in depth comparison of the drivecycles has been published previously in [37].

Figure A1. NEDC drivecycle.

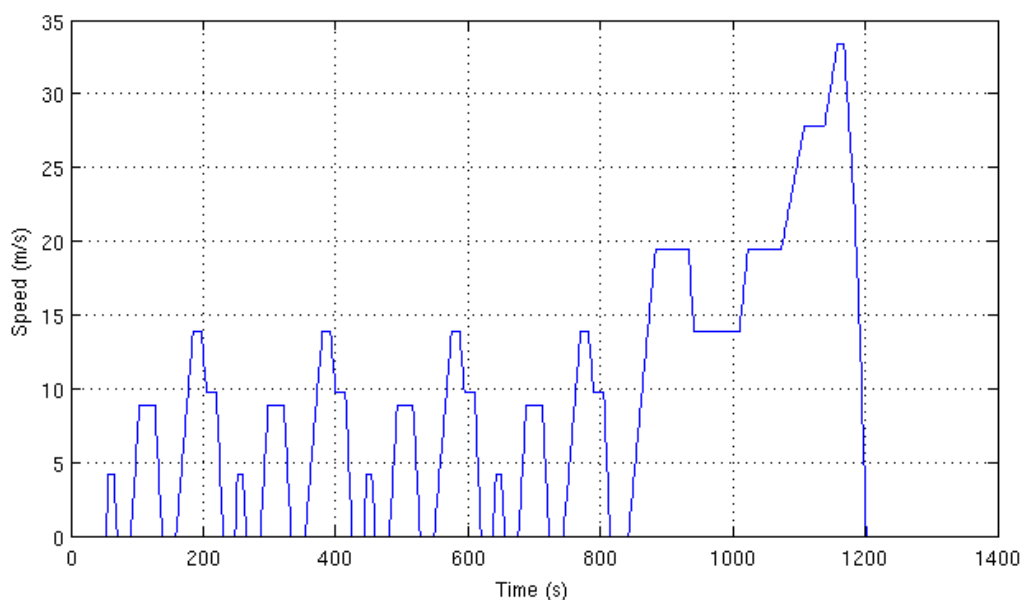


Figure A2. Real-world drivecycle.

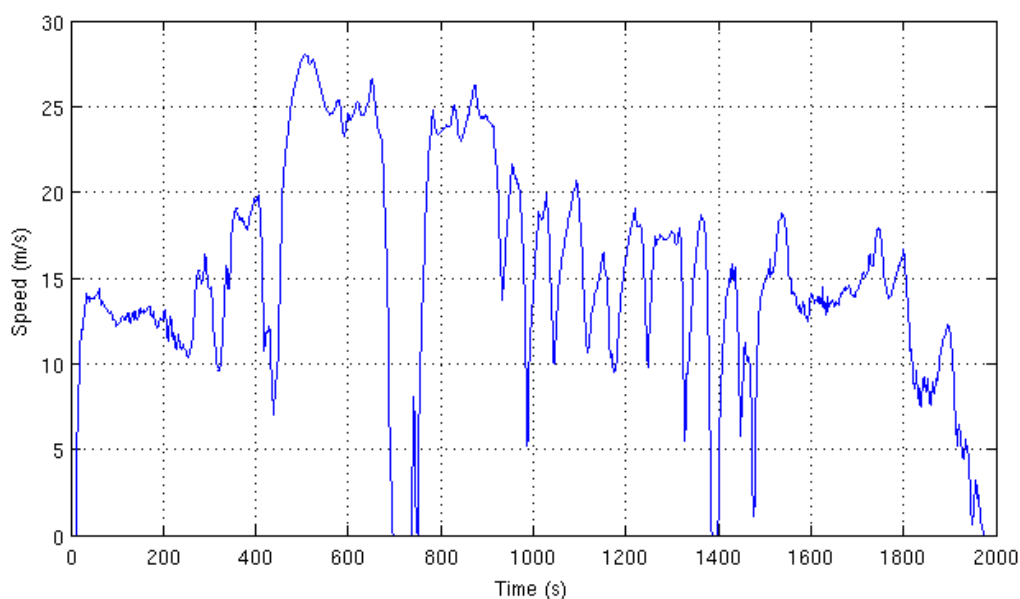
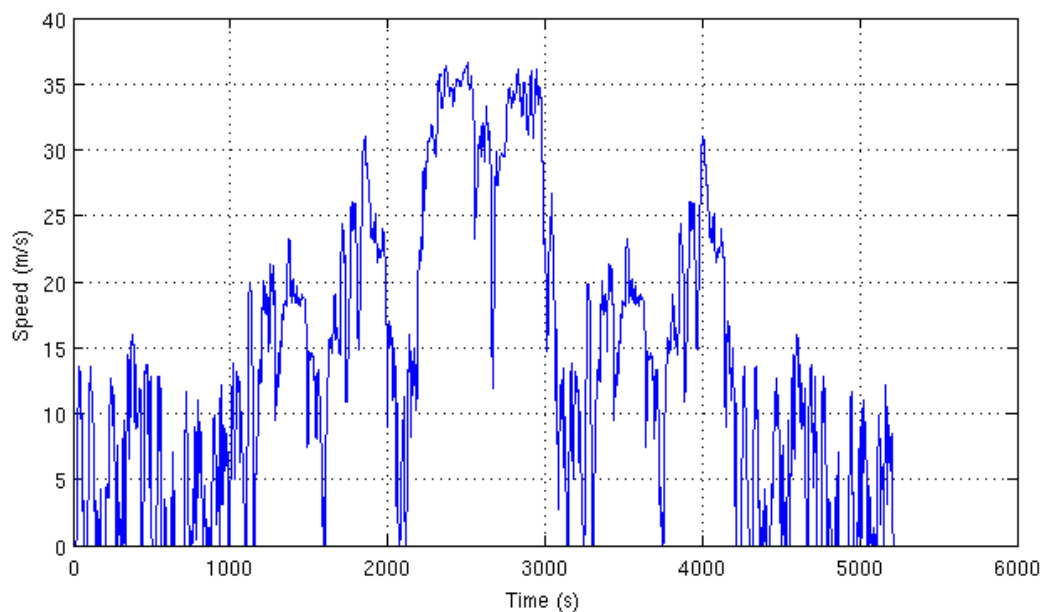


Figure A3. Artemis drivecycle.

A2. Trial Programme

The real-world usage data employed as the foundation for this study was recorded within the UK as part of the Smart Move 2 Electric Vehicle Trial [38]. The evaluation program is part-funded by the UK Department for Business, Innovation and Skills (BIS). The aim of the Smart Move 2 Electrical Vehicle Trial is to further study the performance and acceptance of EVs within both public and private sector fleets. It is beyond the scope of this paper, to discuss the evaluation program in detail. A summary of pertinent data is provided for reference in Table A1, with further information being available from previously published work [39]. During the course of the program, whenever an EV was driven, key vehicle parameters were automatically recorded from the vehicles Controller Area Network or CAN bus and uploaded to a central database for analysis. With respect to the research reported here, the data from the seven Smart Electric Drive (ED) vehicles is employed as the primary focus of the modeling and optimization activity.

Table A1. Smart Move 2 Trial Program Details.

Trial program parameters	Data
Duration of Program	November 2010–March 2011
Number of vehicles	8
Types of Vehicles	7 Smart EVs and 1 Mitsubishi i-Miev
Total kilometers driven by Smart EVs during program	4268 km
Number of demonstration days	12
Number of participating organizations	5

The Smart ED is an EV designed primarily for deployment within urban areas. It has 16.5 kWh Lithium Ion battery, with a peak power rating of 30 kW during discharge and 10 kW for charge. The unladen mass of the vehicle has been measured as 965 kg. An integrated single-phase 3.3 kW on-board charger enables recharging of the HV battery at both the 220 V and 110 V levels. The vehicle's

controller limits the top speed of the vehicle to 100 km/h. The range of the vehicle, published by the manufacturer over the new European driving cycle (NEDC) cycle, is 135 km [15].

Conversely within the US, the Environmental Protection Agency (EPA) states the vehicle's official electric range as 101 km. Figure A4 presents a schematic representation of the EV powertrain, while Table A2 summarizes the pertinent data recorded from the EVs during their use.

Figure A4. Layout of the EV Powertrain.

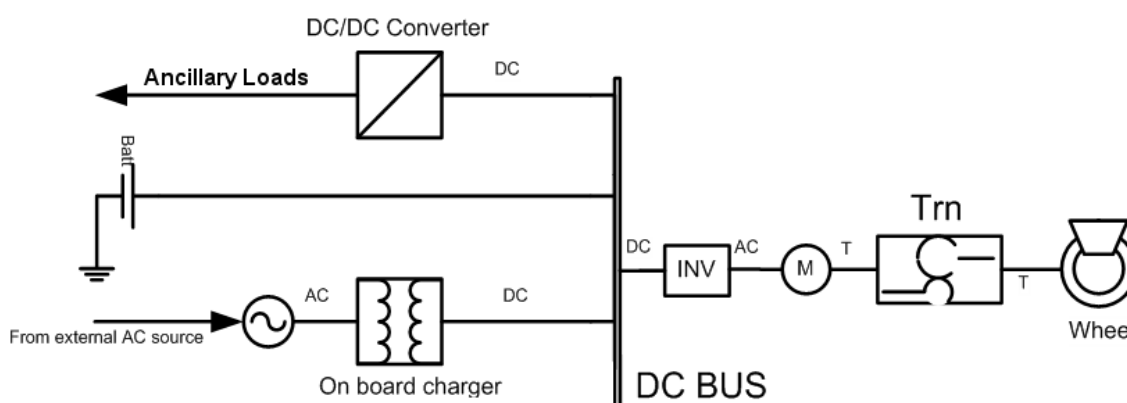


Table A2. Data recorded from each of the EVs.

Vehicle Parameter	Unit	Description
Battery voltage	V	Terminal voltage of the HV battery
Battery current	A	Battery current measured at the terminals of the battery pack
Machine speed	Rad/s	Rotational velocity of the electrical machine
Machine voltage	V	DC voltage, measured at the input to the inverter
Machine current	A	Machine current measured at the terminals of the inverter
Auxiliary power	kW	Power consumed by ancillary devices, including power steering and thermal management of the cabin and battery pack
Charger voltage	V	AC mains voltage measured by the onboard charger
Charger current	A	AC Mains current measured by the onboard charger
Battery temperature	°C	Individual measurement of battery pack temperature

References

1. Chan, C.C. The state of the art of electric, hybrid, and fuel cell vehicles. *Proc. IEEE* **2007**, *95*, 704–718.
2. Douglas, C.; Stewart, A. *Influences on the Low Carbon Car Market from 2020–2030*; Final Report 2011; Report for Low Carbon Vehicle Partnership: Cambridge, UK, 2011.
3. Franke, T.; Neumann, I.; Bühler, F.; Cocron, P.; Krems, J.F. Experiencing range in an electric vehicle: Understanding psychological barriers. *Appl. Psychol.* **2012**, *61*, 368–391.
4. Markel, T.; Simpson, A. Plug-In Hybrid Electric Vehicle Energy Storage System Design. In *Proceedings of the Advanced Automotive Battery Conference*; Baltimore, MD, USA, 17–19 May 2006; pp. 1–9.

5. Patil, R.; Adornato, B.; Filipi, Z. Impact of Naturalistic Driving Patterns on PHEV Performance and System Design. In *Proceedings of the SAE 2009 Powertrains Fuels and Lubricants Meeting*, San Antonio, TX, USA, 2 November 2009; SAE Technical Paper 2009-01-2715.
6. Shiau, C.N.; Samaras, C.; Hauffe, R.; Michalek, J.J. Impact of battery weight and charging patterns on the economic and environmental benefits of plug-in hybrid vehicles. *Energy Policy* **2009**, *37*, 2653–2663.
7. Kammen, D.M.; Arons, S.M.; Lemoine, D.; Hummel, H. *Cost-Effectiveness of Greenhouse Gas Emission Reductions from Plug-in Hybrid Electric Vehicles*; Working Paper No. GSPP08-014; Goldman School of Public Policy: Berkeley, CA, USA, 2008.
8. Moura, S.J.; Callaway, D.S.; Fathy, H.K.; Stein, J.L. Impact of battery sizing on stochastic optimal power management in plug-in hybrid electric vehicles. In *Proceedings of the IEEE International Conference on Vehicular Electronics and Safety*; Columbus, OH, USA, 22–24 September 2008; pp. 96–102.
9. Tulpule, P.; Marano, V.; Rizzoni, G. Effects of different PHEV Control Strategies on Vehicle Performance. In *Proceedings of the American Control Conference*, St. Louis, MO, USA, 10 June 2009; pp. 3950–3955.
10. Karbowski, D. Impact of Component Size on Plug-In Hybrid Vehicle Energy Consumption Using Global Optimization In *Proceedings of the 23rd International Electric Vehicle Symposium (EVS23)*, Anaheim, CA, USA, 2 December 2007.
11. Shankar, R.; Marco, J.; Assadian, F. Design of an Optimized Charge-Blended Energy Management Strategy for a Plug-in Hybrid Vehicle. In *Proceedings of the UKACC (United Kingdom Automatic Control Council) International Conference on Control*, Cardiff, UK, 3–5 September 2012; pp. 1–6.
12. Dextreit, C.; Assadian, F.; Kolmanovsky, I.; Mahtani, J.; Burnham, K. Hybrid Electric Vehicle Energy Management Using Game Theory In *Proceedings of the SAE World Congress & Exhibition*, Detroit, MI, USA, 14 April 2008; SAE Technical Paper 2008-01-1317.
13. Shankar, R.; Marco, J.; Assadian, F. A methodology to Determine Drivetrain Efficiency Based on External Environment. In *Proceedings of the IEEE International Electric Vehicle Conference (IEVC)*, Greenville, SC, 4–8 March USA, 2012; pp. 1–6.
14. Smart Electric Drive Homepage. Available online: <http://uk.smart.com/> (accessed on 16 November 2011).
15. Wu, X.; Cao, B.; Li, X.; Xu, J.; Ren, X. Component sizing optimization of plug-in hybrid electric vehicles. *Appl. Energy* **2011**, *88*, 799–804.
16. Zytec IDT 120-55 Integrated 55 kW Electric Engine. Available online: <http://www.zytekautomotive.co.uk/Products/ElectricEngines/55kW.aspx> (accessed on 16 November 2012).
17. Tremblay, O.; Dessaint, L.; Dekkiche, A. A Generic Battery Model for the Dynamic Simulation of Hybrid Electric Vehicles. In *Proceedings of the IEEE Vehicle Power and Propulsion Conference*, Arlington, TX, USA, 9 September 2007.
18. Rizzoni, G.; Guzzella, L.; Baumann, B.M. Unified modeling of hybrid electric vehicle drivetrains. *Mechatronics* **1999**, *4*, 246–257.
19. Guzzella, L.; Sciarretta, A. *Vehicle Propulsion Systems: Introduction to Modeling and Optimization*; Springer-Verlag: Berlin, Germany, 2005.

20. Silva, C.; Ross, M.; Farias, T. Evaluation of energy consumption, emissions and cost of plug-in hybrid vehicles. *Energy Convers. Manag.* **2009**, *50*, 1635–1643.
21. Simpson, A. Cost-Benefit Analysis of Plug-in Hybrid Electric Vehicle Technology. In *Proceedings of the 22nd International Battery, Hybrid and Fuel Cell Electric Vehicle Symposium and Exhibition (EVS-22)*, Yokohama, Japan, 23 October 2006.
22. O’Keefe, M.; Brooker, A.; Johnson, C.; Mendelsohn, M.; Neubauer, J. Battery Ownership Model: A Tool for Evaluating the Economics of Electrified Vehicles and Related Infrastructure. In *Proceedings of the 25th International Battery, Hybrid and Fuel Cell Electric Vehicle Symposium and Exposition*, Shenzhen, China, 5 November 2010.
23. Paganelli, G.; Guerra, T.M.; Delprat, S.; Santin, J.J.; Delhom, M.; Combes, E. Simulation and assessment of power control strategies for a parallel hybrid car. *J. Automob. Eng.* **2000**, *214*, 705–717.
24. Serrao, L.; Onori, S.; Rizzoni, G. ECMS as a realization of Pontryagin’s minimum principle for HEV control. In *Proceedings of the IEEE American Control Conference*, St. Louis, MO, USA, 10 June 2009; pp. 3964–3969.
25. Zhang, C.; Vahidi, A.; Pisu, P.; Li, X.; Tennent, K. Role of terrain preview in energy management of hybrid electric vehicles. *IEEE Trans. Veh. Tech.* **2009**, *59*, pp 1139–1147.
26. Pisu, P.; Rizzoni, G. A comparative study of supervisory control strategies for hybrid electric vehicles. *IEEE Trans. Control Syst. Tech.* **2007**, *15*, 506–518.
27. Musardo, C.; Rizzoni, G.; Staccia, B. A-ECMS: An Adaptive Algorithm for Hybrid Electric Vehicle Energy Management. In *Proceedings of 44th IEEE Conference on Decision and Control*, Seville, Spain, 12 December 2005; pp. 1816–1823.
28. Stamps, A.T.; Holland, C.E.; White, R.E.; Gatzke, E.P. Analysis of capacity fade in a lithium ion battery. *J. Power Sources* **2005**, *150*, 229–239.
29. Kai, L.C.; Li, P.Y.; Chase, T.R. Optimal Design of Power-Split Transmissions for Hydraulic Hybrid Passenger Vehicles. In *Proceedings of the IEEE American Control Conference (ACC)*, San Francisco, CA, USA, 29 June 2011; pp. 3295–3300.
30. Lagarias, J.; Reeds, J.; Wright, M.; Wright, P. Convergence properties of the Nelder–Mead simplex method in low dimensions. *SIAM J. Optim.* **1998**, *9*, 112–147.
31. Liaw, B.Y.; Dubarry, M. From driving cycle analysis to understanding battery performance in real-life electric hybrid vehicle operation. *J. Power Sources* **2007**, *174*, 76–88.
32. Smith, K.; Wang, C. Power and thermal characterization of a lithium-ion battery pack for hybrid-electric vehicles. *J. Power Sources* **2006**, *160*, 662–673.
33. Alkidas, A.C. Combustion advancements in gasoline engines. *Energy Convers. Manag.* **2007**, *48*, 2751–2761.
34. Regulation 101—Battery electric vehicles with regard to specific requirements for construction and functional safety. Available online: <http://www.unece.org/trans/main/wp29/wp29regs101-120.html> (accessed on 16 November 2012).
35. Emission factors for company reporting. Available online: <http://www.defra.gov.uk/publications/files/pb13792-emission-factor-methodology-paper-120706.pdf> (accessed on 16 November 2012).

36. Marano, V.; Onori, S.; Guezennec, Y.; Rizzoni, G.; Madella, N. Lithium-ion batteries life estimation for plug-in hybrid electric vehicles. In *Proceedings of the IEEE Vehicle Power and Propulsion Conference*, Dearborn, MI, USA, 7 November 2009; pp. 536–543.
37. Shankar, R.; Marco, J.; Assadian, F. A method for estimating the energy consumption of electric vehicles and plug-in hybrid electric vehicles under real-world driving conditions. *IET Intell. Transp. Syst.* **2012**, submitted for publication.
38. Carroll, S.; Walsh, C. The smart move trial description and initial results. Available online: <http://www.cenex.co.uk/resources> (accessed on 16 November 2012).
39. Shankar, R.; Marco, J. Performance of an EV during real-world usage. In *Proceedings of the Hybrid Electric Vehicle Conference*, Coventry, UK, 18 May 2011.

© 2012 by the authors; licensee MDPI, Basel, Switzerland. This article is an open access article distributed under the terms and conditions of the Creative Commons Attribution license (<http://creativecommons.org/licenses/by/3.0/>).